Research Article

Check for updates

Transition from isotropic positive to negative thermal expansion by local Zr_6O_8 node distortion in MOF-801

Rui Ma[1], Zhanning Liu[2], Liang Chen[1], Qiang Li[1], Kun Lin[1] , Xin Chen[1], Jinxia Deng[1], Koji Ohara[3], Xianran Xing[1]

[1]Beijing Advanced Innovation Center for Materials Genome Engineering, Institute of Solid State Chemistry, University of Science and Technology Beijing, Beijing 100083, China.
[2]School of Materials Science and Engineering, Shandong University of Science and Technology, Qingdao 266590, Shandong, China.
[3]Diffraction and Scattering Division, Center for Synchrotron Radiation Research, Japan Synchrotron Radiation Research Institute, Sayo-cho, Sayo-gun, Hyogo 679-5198, Japan.

Correspondence to: Prof. Xianran Xing, Department of Physical Chemistry, University of Science and Technology Beijing, Xueyuan Rd. 30, Haidian District, Beijing 100083, China. E-mail: xing@ustb.edu.cn; Dr. Zhanning Liu, School of Materials Science and Engineering, Shandong University of Science and Technology, Qingdao 266590, Shandong, China. E-mail: znliu@sdust.edu.cn

Abstract

The chemical designability and diversity of metal-organic frameworks (MOFs) endow them with plenty of anomalous properties, such as negative thermal expansion (NTE). Herein, we investigated the thermal expansion behaviors of the well-known MOF-801, which has been widely used in water adsorption and gas separation. The analyses of variable temperature powder X-ray diffraction and Rietveld refinements revealed a fascinating transition from positive thermal expansion to NTE. Further *in situ* Raman spectra and pair distribution function investigations shed light on the transition being attributed to the local Zr_6O_8 node distortion rather than a long-range phase transition. Our findings will enhance the comprehension of NTE and contribute to the effective utilization of MOF-801 over a broad temperature range.

Keywords: MOF-801, negative thermal expansion (NTE), pair distribution function (PDF), local structure, Zr_6O_8 node distortion

INTRODUCTION

Thermal expansion, as an inherent physical property, significantly influences the performance and lifetime of materials. Consequently, designing smart materials with tunable or switchable thermal expansion properties is a significant yet challenging pursuit for materials scientists. The emergence of negative thermal expansion (NTE) materials presents a promising prospect[1,2]. Generally, the coefficients of thermal expansion (CTEs) can be modified by precisely controlling the chemical substitution[3]. For instance, substituting Sc^{3+} with isovalent but smaller radius cations such as Ga^{3+} or Fe^{3+} can induce local distortions, resulting in a continuous transition from NTE to positive thermal expansion (PTE)[4]. In the $(Sc,Ti)Fe_2$-based intermetallic, a crossover from typical PTE observed in $ScFe_2$ and $TiFe_2$ to a pronounced NTE in $(Sc_{0.4}Ti_{0.6})Fe_2$ was noted, attributed to the unconventional magnetovolume effect[5]. Furthermore, NTE materials can be composited with positive ones, bringing about a series of multifunctional materials. For example, the composite of $Mn_{0.6}Fe_{0.4}NiGe_{0.5}Si_{0.5}$ with In not only exhibits tunable thermal expansion but also demonstrates excellent machinability and heat transfer performance[6].

Metal-organic frameworks (MOFs), a class of innovative porous materials constructed from inorganic metal nodes and organic linkers, have recently been recognized as an ideal platform for studying NTE[7-9]. The structural design flexibility and ease of decoration characteristics are expected to expand the range of NTE materials, offering additional strategies for tailoring CTEs[10]. To date, several MOFs have reported to exhibit NTE, such as IRMOF-1[11], HKUST-1[12], UiO-66(Hf)[13], MIL-68(In)[14], NU-1000(Zr)[15], Cd_sq[16], Cd(trz)Cl[17], and so on. A common characteristic of these MOFs is their construction using units with high symmetry, such as linear, triangular or square configurations. This structural feature imparts the framework with significant quantities of low-frequency phonons[18,19]. Upon heating, the transverse vibration, rotation or flipping tends to drag the connected nodes closer, resulting in the manifestation of NTE[20]. The close relationship between the ligand vibration and NTE suggests that introducing guest solvents or gases can effectively tailor NTE due to the steric hindrance effect[21-23]. Additionally, steric hindrance groups can be directly decorated as side groups of the ligands[24,25]. In addition to decorating organic ligands, the inorganic nodes, serving as pivotal elements within the framework, have been suggested to play a crucial role in determining lattice vibration behaviors. For example, the spin state of hexanuclear $Fe^{III}_4Fe^{II}_2$ significantly influences the geometric configuration of the framework and the spin crossover can induce a colossal thermal expansion[26]. Recently, Chen *et al.* and Platero-Prats *et al.* discovered that the 8-connected Zr_6O_8 nodes can undergo local distortion upon heating, which can also contribute to the NTE[15,27].

In this research, we chose to investigate the thermal expansion property of MOF-801, which is composed of "zig-zag" type dicarboxylate ligands and Zr_6O_8 nodes[28]. Considering the widespread applications of the MOF-801 in gas separation and water adsorption[29-32], a detailed understanding of how the lattice and structure change upon heating (and cooling) will be useful for modifying its actual performance.

MATERIALS AND METHODS

MOF-801 samples were prepared and activated according to synthesis procedures as reported[28,33,34]. A mixture of $ZrOCl_2 \cdot 8H_2O$ (0.23 g, 0.70 mmol) and fumaric acid (0.081 g, 0.70 mmol) was dissolved in N,N-Dimethylformamide (DMF) within a 50-mL screw-capped glass jar, and 5.3 mL formic acid was added into the solution; then, the mixture was heated at 393 K for 24 h. The powder product was washed at least twice using water and alcohol and then dried at 383 K to obtain a white powder for subsequent experiment measurements. Prior to variable temperature X-ray powder diffraction (XRD), the powder sample was *in situ* dried at 383 K for 2 h to completely remove the adsorbed water molecules. Temperature-dependent X-ray diffraction (Cu-K_α = 1.54056 Å) data was collected using a PANalytical X'Pert PRO. All Rietveld refinements were performed by the GSAS and EXPGUI program[35]. Raman spectra were acquired with

LabRAM HR Evolution, Horiba. *In situ* X-ray total-scattering data suitable for pair distribution function (PDF) and diffraction analyses were collected at the beamline of BL08W at the Super Photon ring-8 (SPring-8) facility in Japan. The samples, in powder form, were loaded into 1 mm-diameter capillaries and were tested over a temperature range of 100 to 500 K with 25 K intervals under atmospheric conditions. The PDF patterns, denoted as G(r), were extracted from X-ray total scattering data (λ = 0.6597 Å) using xPDFsuite up to a Q_{max} value of 20 Å^{-1}[36].

RESULTS AND DISCUSSION

MOF-801, Zr_6O_8(fumarate)$_6$, is constructed by Zr_6O_8 nodes and fumaric acid ligands [Figure 1A-C]. The Zr_6O_8 node contains six zirconium atoms with μ_3-O moieties coordinating at each face. The metal coordination is further completed by 12 carboxylate donor groups, which bridge the metal atoms along the octahedral edges. Furthermore, these 12-connected metal clusters are connected by fumarate ligands to form a three-dimensional cubic lattice with the *fcu* (face-centered cubic) topology (*P n*-3, a = 17.83480 Å). Structure arrangement in MOF-801 bears a resemblance to archetypal members of the extensively studied iso-reticular series of "UiO" MOFs, which also feature the Zr_6O_8 node but use different dicarboxylate ligands[37]. Considering the broad temperature range of MOF-801 potential applications, there is considerable interest in understanding its thermal expansion characteristic.

To investigate the thermal expansion behavior of MOF-801, *in situ* variable temperature X-ray diffraction analyses were used [Supplementary Figure 1]. As shown in Figure 2A, upon heating from 100 to 500 K, an obvious peak shift (particularly in the high temperature range) toward high angles was observed, inferring lattice contraction according to the Bragg equation. Subsequently, when cooling from 500 to 100 K, a peak shift toward a low angle value can also be observed. To precisely reveal the lattice changes, Rietveld refinements were performed and the results are shown in Figure 2B and Supplementary Figure 2. From 100 to 375 K, the lattice parameter *a* monotonously expands with the coefficient α_a = +4.30(7) MK^{-1}. The contradictory result between the Rietveld refinements and observed peak shifts is due to the height of sample stage changes. Evidently, the thermal expansion behavior is different from previously reported Zr_6O_8-based analogs. Those MOFs constructed from linear dicarboxylates, such as 1,4-benzenedicarboxylic acid and 4,4′-(ethyne-1,2-diyl)dibenzoic acid, tend to show monotonous NTE owing to the transverse vibration of ligands[13,38], while, here, we found that the MOF-801 shows normal PTE. This may be caused by the unique "zig-zag" configuration of the fumarate ligand that can frustrate the correlated vibrations. Noticeably, in the high temperature range (375-500 K), *a* dramatically contracts with the coefficient α_a = -31.6(1) MK^{-1}, which exceeds most of the reported NTE materials and is close to the value of UiO-66(Hf) (α_a = -32.3 MK^{-1}, Supplementary Table 1)[13]. In contrast to UiO-66(Hf), the transition between NTE and PTE in MOF-801 still exists in the subsequent cooling treatment. Moreover, the second cycling variable temperature measurement showed a similar trend of changes, although the magnitude of change was much smaller. This indicates that the transition between PTE and NTE is reversible to some extent. Noticeably, through the entire *in situ* variable temperature diffraction measurements, no discernible appearance or emergence of peaks was observed, except for slight shifts. This suggests the absence of any long-range phase transitions. Moreover, all the Rietveld refinements fit well based on the previously reported structure [Supplementary Figure 2]. The weakened magnitude of NTE for the subsequent cooling and cycling measurements may be caused by the defect-induced thermal densification similar to the UiO-66(Hf)[13].

For framework materials, the NTE is generally believed to be associated with low frequency phonons[18,39,40]. To gain a deeper insight into the vibration modes of MOF-801, *in situ* variable temperature Raman spectroscopy investigation was conducted across a temperature range of 125-475 K with 25 K internals [Figure 3A]. Throughout the entire temperature range, no noticeable blue shift was observed for the low
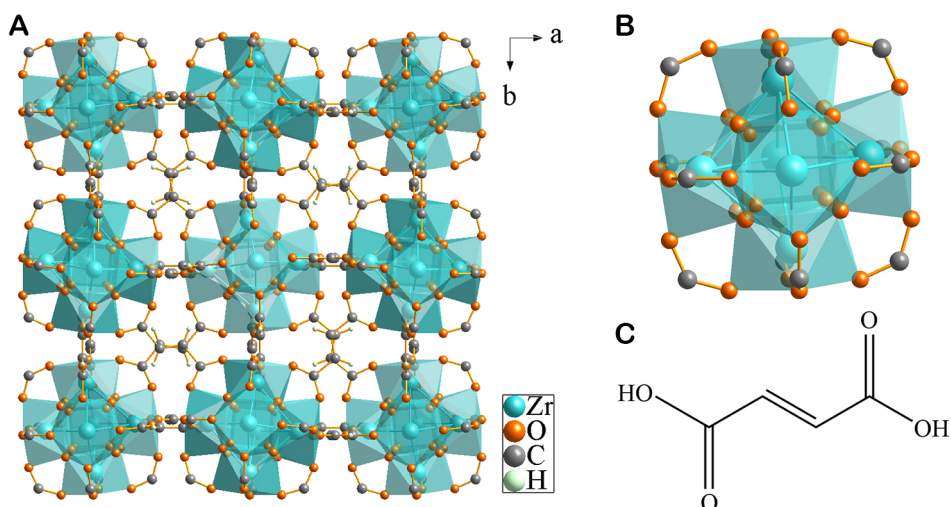
Figure 1. (A) Illustration of the crystal structure of MOF-801 viewed along the *c*-axis. (B) The structure of 12-connected Zr_6O_8 node in MOF-801 (Zr: blue, O: orange, C: grey, H: light green). (C) Chemical structure of the fumaric acid ligand.
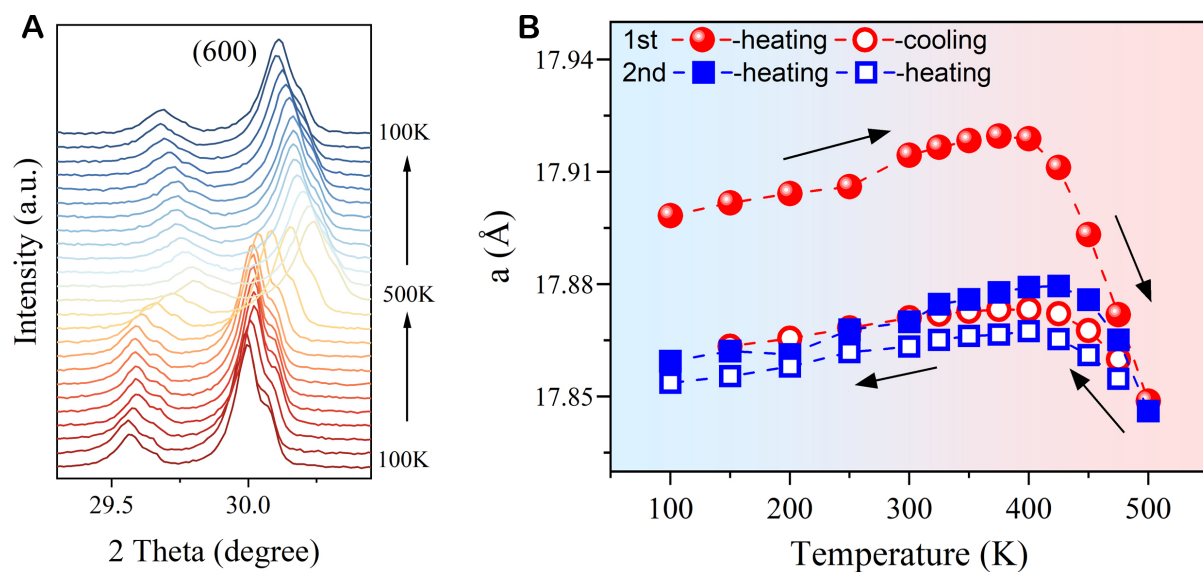

Figure 2. (A) The zoomed temperature-dependent X-ray diffraction profiles of MOF-801. (B) The unit cell parameters of MOF-801 with temperatures. Color code: first cycle, red; second cycle, blue. The symbols corresponding to the heating and cooling processes are shown as filled and empty scatters, respectively.

frequency bands (< 200 cm^{-1}, Figure 3B). The high frequency vibration bands corresponding to the carboxylate stretching $v_{as}(COO)$, $v_s(COO)$ and -CH_2 wagging also show similar trends [Supplementary Figure 3][41], indicating that the anomalous PTE to NTE transition may not be attributed to the transverse vibration of ligands.

Both the *in situ* powder X-ray diffraction and Raman spectroscopy indicated the absence of a phase transition in the long-range of the structure. With the concern of how the local structure changes, we performed PDF analysis based on the high-resolution X-ray total scattering. The PDF patterns predominantly feature atom-atom correlations, primarily focusing on the strongly scattering Zr atoms [Figure 4A]. This includes the Zr-O bond at distance of ~2.2 Å (path 1, Figure 4B), the Zr···Zr distances as
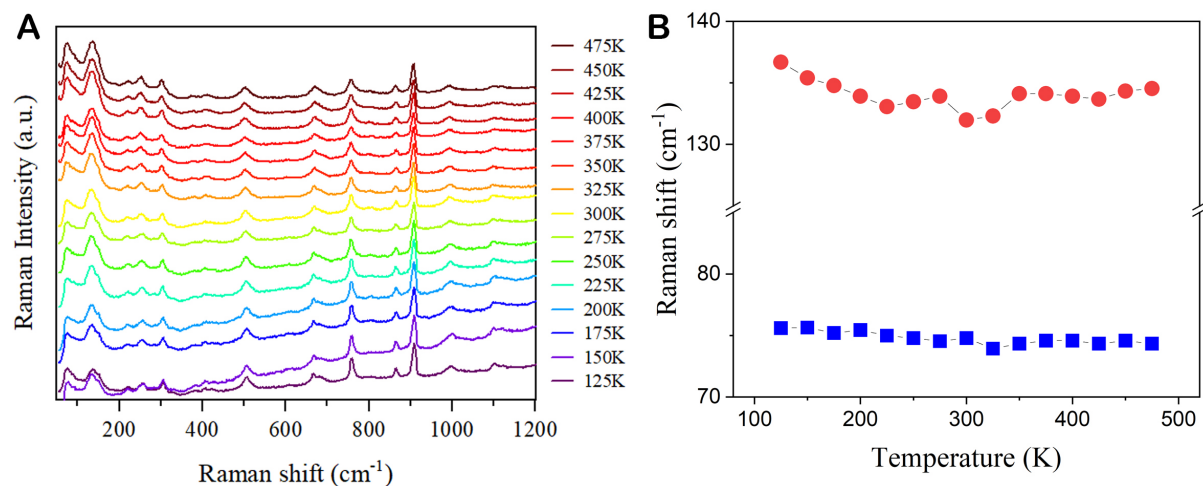
Figure 3. (A) *In situ* variable temperature Raman spectra of MOF-801. (B) Representative low-frequency Raman band shifts of MOF-801 *vs.* temperature.
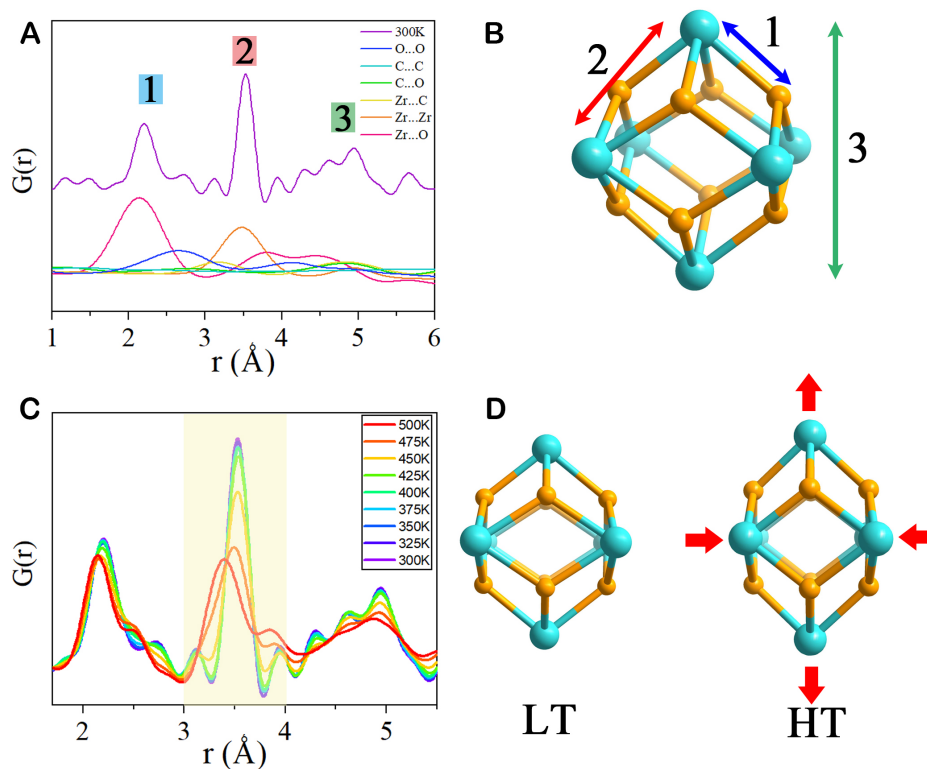

Figure 4. (A) PDF patterns of MOF-801 at 300 K (path 1: Zr-O atom pair, path 2: Zr⋯Zr atom pair, path 3: Zr⋯Zr atom pair). (B) Schematic diagram of the Zr_6O_8 node, showing paths 1, 2 and 3, respectively. (C) Temperature-dependent PDF patterns in the range of 1.5-5.5 Å. (D) Illustration of the local Zr_6O_8 node distortion with temperature.

the edges of the Zr_6 octahedron at distance of ~3.5 Å (path 2) and as the two diagonal sites at distance of ~5.0 Å (path 3). The observed single Zr⋯O distances involve contributions from overlapping Zr-carboxylate and Zr-oxo distances. The singular Zr⋯Zr distance at 3.5 Å corresponds to the 12 equivalent Zr⋯Zr distances within the regular octahedron, highlighting the structural intricacies of MOF-801 at the local level.

Before 375 K, no obvious peak changes, including peak intensity and position, can be observed, while a noticeable alteration in the local structure becomes evident when the temperature exceeds 375 K. As shown in Figure 4C, the initially singular peak at ~3.5 Å that corresponds to the Zr⋯Zr pair splits into two peaks at 3.3 and 3.8 Å with an intensity ratio of nearly 2:1. The peak at ~5 Å also broadens, indicating a wider distribution of Zr⋯Zr distances and disorder. These changes of Zr⋯Zr pairs suggest that the originally regular Zr_6 octahedron become distorted Figure 4D, consistent with a recently reported 8-connected Zr_6O_8 node in NU-1000 that capped with H_2O or OH[15]. As discussed by Chen *et al.*, this type of distortion behavior possesses relatively lower reversibility, which may be the origin of difference between the first and second cycling measurements[15]. To quantify the distortion extent in the local structure, the change in the crucial Zr⋯O distance was evaluated. As shown in Supplementary Figure 4, the change of Zr⋯O distance aligns with the trend observed in the CTEs depicted in Figure 2B. So, we have reason to believe that the distorted Zr_6O_8 nodes possess a smaller volume, giving rise to observed volume contraction at high temperatures.

CONCLUSIONS

In summary, we investigated the thermal expansion behavior of MOF-801, a significant representative of typical Zr-based MOFs. In the low temperature range (< 375 K), it exhibits normal PTE due to the transverse vibration of dicarboxylate ligands being frustrated by the "zig-zag" configuration of fumarate ligands. Intriguingly, a distinctive transition from PTE to NTE was identified in the temperature range of 375~500 K. Detailed analyses through *in situ* powder X-ray diffraction and Raman spectroscopy analysis excluded the occurrence of long-range phase transitions. The PDF study unveiled a temperature-induced local distortion of the Zr_6O_8 node, contributing to the occurrence of NTE. This sheds light on the dynamics of the local structure within a specific temperature range, enhancing our understanding of NTE. The current observation of NTE in MOF-801 holds promise for exploring diverse potential applications.

DECLARATIONS

Authors' contributions
Conceived and designed the study: Xing X
Prepared the samples and collected the data: Ma R
Analyzed data and wrote the main draft of the paper: Ma R, Liu Z, Xing X
Examined the thermal expansion results: Chen L, Li Q, Lin K, Chen X, Deng J
Conducted the Synchrotron radiation measurements: Ohara K, Li Q
All authors discussed the results and commented on the manuscript.

Availability of data and materials
Not applicable.

Conflicts of interest
All authors declared that there are no conflicts of interest.

Ethical approval and consent to participate
Not applicable.

Consent for publication
Not applicable.

Copyright
© The Author(s) 2024.

REFERENCES

1. Li Q, Lin K, Liu Z, et al. Chemical diversity for tailoring negative thermal expansion. *Chem Rev* 2022;122:8438-86. DOI
2. Takenaka K. Negative thermal expansion materials: technological key for control of thermal expansion. *Sci Technol Adv Mater* 2012;13:013001. DOI PubMed PMC
3. Chen J, Hu L, Deng J, Xing X. Negative thermal expansion in functional materials: controllable thermal expansion by chemical modifications. *Chem Soc Rev* 2015;44:3522-67. DOI PubMed
4. Hu L, Chen J, Fan L, et al. Zero thermal expansion and ferromagnetism in cubic $Sc_{1-x}M_xF_3$ (M = Ga, Fe) over a wide temperature range. *J Am Chem Soc* 2014;136:13566-9. DOI
5. Song Y, Sun Q, Xu M, et al. Negative thermal expansion in (Sc,Ti)Fe$_2$ induced by an unconventional magnetovolume effect. *Mater Horiz* 2020;7:275-81. DOI
6. Zhou H, Tao K, Chen B, et al. Low-melting metal bonded MM'X/In composite with largely enhanced mechanical property and anisotropic negative thermal expansion. *Acta Mater* 2022;229:117830. DOI
7. Balestra SR, Bueno-Perez R, Hamad S, Dubbeldam D, Ruiz-Salvador AR, Calero S. Controlling thermal expansion: a metal-organic frameworks route. *Chem Mater* 2016;28:8296-304. DOI PubMed PMC
8. Zhang JP, Zhou HL, Zhou DD, Liao PQ, Chen XM. Controlling flexibility of metal-organic frameworks. *Nat Sci Rev* 2018;5:907-19. DOI
9. Burtch NC, Baxter SJ, Heinen J, et al. Negative thermal expansion design strategies in a diverse series of metal-organic frameworks. *Adv Funct Mater* 2019;29:1904669. DOI
10. Schneider C, Bodesheim D, Ehrenreich MG, et al. Tuning the negative thermal expansion behavior of the metal-organic framework Cu_3BTC_2 by retrofitting. *J Am Chem Soc* 2019;141:10504-9. DOI
11. Dubbeldam D, Walton KS, Ellis DE, Snurr RQ. Exceptional negative thermal expansion in isoreticular metal-organic frameworks. *Angew Chem Int Ed* 2007;46:4496-9. DOI PubMed
12. Wu Y, Kobayashi A, Halder GJ, et al. Negative thermal expansion in the metal-organic framework material $Cu_3(1,3,5-$benzenetricarboxylate)$_2$. *Angew Chem Int Ed* 2008;47:8929-32. DOI
13. Cliffe MJ, Hill JA, Murray CA, Coudert FX, Goodwin AL. Defect-dependent colossal negative thermal expansion in UiO-66(Hf) metal-organic framework. *Phys Chem Chem Phys* 2015;17:11586-92. DOI PubMed
14. Liu Z, Li Q, Zhu H, et al. 3D negative thermal expansion in orthorhombic MIL-68(In). *Chem Commun* 2018;54:5712-5. DOI
15. Chen Z, Stroscio GD, Liu J, et al. Node distortion as a tunable mechanism for negative thermal expansion in metal-organic frameworks. *J Am Chem Soc* 2023;145:268-76. DOI
16. Liu Z, Ma R, Deng J, Chen J, Xing X. Molecular packing-dependent thermal expansion behaviors in metal squarate frameworks. *Chem Mater* 2020;32:2893-8. DOI
17. Liu Z, Fan L, Xing C, Wang Z. Negative thermal expansion in the noncarboxylate based metal-organic framework Cd(trz)Cl. *ACS Mater Lett* 2023;5:1911-5. DOI
18. Zhou W, Wu H, Yildirim T, Simpson JR, Walker ARH. Origin of the exceptional negative thermal expansion in metal-organic framework-5 $Zn_4O(1,4$-benzenedicarboxylate)$_3$. *Phys Rev B* 2008;78:054114. DOI
19. Rimmer LH, Dove MT, Goodwin AL, Palmer DC. Acoustic phonons and negative thermal expansion in MOF-5. *Phys Chem Chem Phys* 2014;16:21144-52. DOI PubMed
20. Lock N, Wu Y, Christensen M, et al. Elucidating negative thermal expansion in MOF-5. *J Phys Chem C* 2010;114:16181-6. DOI
21. Goodwin AL, Chapman KW, Kepert CJ. Guest-dependent negative thermal expansion in nanoporous prussian blue analogues $M^{II}Pt^{IV}(CN)_6 \cdot x\{H_2O\}$ (0 ≤ x ≤ 2; M = Zn, Cd). *J Am Chem Soc* 2005;127:17980-1. DOI
22. Zhou HL, Zhang YB, Zhang JP, Chen XM. Supramolecular-jack-like guest in ultramicroporous crystal for exceptional thermal expansion behaviour. *Nat Commun* 2015;6:6917. DOI PubMed PMC
23. Auckett JE, Barkhordarian AA, Ogilvie SH, et al. Continuous negative-to-positive tuning of thermal expansion achieved by controlled gas sorption in porous coordination frameworks. *Nat Commun* 2018;9:4873. DOI PubMed PMC
24. Baxter SJ, Schneemann A, Ready AD, Wijeratne P, Wilkinson AP, Burtch NC. Tuning thermal expansion in metal-organic frameworks using a mixed linker solid solution approach. *J Am Chem Soc* 2019;141:12849-54. DOI PubMed
25. Henke S, Schneemann A, Fischer RA. Massive anisotropic thermal expansion and thermo□responsive breathing in metal-organic frameworks modulated by linker functionalization. *Adv Funct Mater* 2013;23:5990-6. DOI

26.　Sun HY, Meng YS, Zhao L, et al. Colossal anisotropic thermal expansion through coupling spin crossover and rhombus deformation in a hexanuclear {$Fe^{III}_4Fe^{II}_2$} Compound. *Angew Chem Int Ed* 2023;62:e202302815.　DOI

27.　Platero-Prats AE, Mavrandonakis A, Gallington LC, et al. Structural transitions of the metal-oxide nodes within metal-organic frameworks: on the local structures of NU-1000 and UiO-66. *J Am Chem Soc* 2016;138:4178-85.　DOI

28.　Furukawa H, Gándara F, Zhang YB, et al. Water adsorption in porous metal-organic frameworks and related materials. *J Am Chem Soc* 2014;136:4369-81.　DOI

29.　Kim H, Rao SR, Kapustin EA, et al. Adsorption-based atmospheric water harvesting device for arid climates. *Nat Commun* 2018;9:1191.　DOI PubMed PMC

30.　Hanikel N, Prévot MS, Yaghi OM. MOF water harvesters. *Nat Nanotechnol* 2020;15:348-55.　DOI PubMed

31.　Xu W, Yaghi OM. Metal-organic frameworks for water harvesting from air, anywhere, anytime. *ACS Cent Sci* 2020;6:1348-54.　DOI PubMed PMC

32.　Iacomi P, Formalik F, Marreiros J, et al. Role of structural defects in the adsorption and separation of C3 hydrocarbons in Zr-fumarate-MOF (MOF-801). *Chem Mater* 2019;31:8413-23.　DOI

33.　Dai S, Nouar F, Zhang S, Tissot A, Serre C. One-step room-temperature synthesis of metal^{IV} carboxylate metal-organic frameworks. *Angew Chem Int Ed* 2021;60:4282-8.　DOI PubMed

34.　Li CN, Wang SM, Tao ZP, et al. Green synthesis of MOF-801(Zr/Ce/Hf) for CO_2/N_2 and CO_2/CH_4 separation. *Inorg Chem* 2023;62:7853-60.　DOI

35.　Toby BH. *EXPGUI*, a graphical user interface for *GSAS. J Appl Cryst* 2001;34:210-3.　DOI

36.　Yang X, Juh'as P, Farrow CL, Billinge SJL. xPDFsuite: an end-to-end software solution for high throughput pair distribution function transformation, visualization and analysis. 2015. Available from: https://arxiv.org/abs/1402.3163 [Last accessed on 12 Apr 2024]. DOI

37.　Cavka JH, Jakobsen S, Olsbye U, et al. A new zirconium inorganic building brick forming metal organic frameworks with exceptional stability. *J Am Chem Soc* 2008;130:13850-1.　DOI

38.　Zhou HL, Bai J, Ye JW, et al. Thermal and gas dual-responsive behaviors of an expanded UiO-66-type porous coordination polymer. *Chempluschem* 2016;81:817-21.　DOI

39.　Zhang X, Jiang X, Molokeev MS, Wang N, Liu Y, Lin Z. Two-dimensional negative thermal expansion in a crystal of $LiBO_2$. *Chem Mater* 2022;34:4195-201.　DOI

40.　Liu Z, Jiang X, Wang C, et al. Near-zero thermal expansion coordinated with geometric flexibility and π-π interaction in anisotropic $[Zn_8(SiO_4)(m\text{-}BDC)_6]_n$. *Inorg Chem Front* 2019;6:1675-9.　DOI

41.　Nijem N, Wu H, Canepa P, et al. Tuning the gate opening pressure of metal-organic frameworks (MOFs) for the selective separation of hydrocarbons. *J Am Chem Soc* 2012;134:15201-4.　DOI